Korean J. Chem. Eng., 32(6), 1194-1200 (2015)
DOI: 10.1007/s11814-014-0289-7

pISSN: 0256-1115
eISSN: 1975-7220

Microstructure and corrosion behavior of electrodeposited nanocrystalline nickel prepared from acetate bath

Ramachandran Sekar†, Kopula Kesavan Jagadesh, and Giri Nagasamy Kuppusamy Ramesh Bapu

Electroplating and Metal Finishing Technology Division, Central Electro Chemical Research Institute, Karaikudi 630 006, Tamil Nadu, India

(*Received 10 April 2014 • accepted 27 September 2014*)

Abstract−The present investigation deals with the electrodeposition of nanocrystalline nickel onto mild steel metallic foil from electrolytes containing nickel acetate as the major metal salt. Two different chlorides, potassium chloride and nickel chloride, were tried for two different baths. Potassium citrate was used as buffer for alternate to boric acid. The additives tried were sodium lauryl sulfate as wetting agent, saccharin as primary brightener and 2-butyne 1,4-diol as secondary brightener. These additives are found to improve the hardness, grain size, surface morphology of the electrodeposited nickel films and throwing power of the nickel acetate electrolytes. The nickel films prepared from nickel chloride containing electrolytes showed higher corrosion resistance as compared to potassium chloride containing electrolytes, because the nickel films produced from the nickel chloride electrolytes are compact and possess fine grained structure. The XRD pattern obtained for electrodeposited nickel shows polycrystalline face centered cubic structure. The crystal size was calculated using Scherrer formula. A uniform and pore free surface was observed under SEM analysis.

Keyswords: Additive, Electrodeposition, SEM Analysis, Crystal Size, XRD, Corrosion

INTRODUCTION

Nickel electrodeposition is one of the most widely used surface finishing processes for decorative, engineering and electroforming applications [1]. In nanocrystalline materials typical dimensions of interest are smaller than 100 nm. Features of nanocrystalline metallic system relevant to the functional properties are grain dimensions, region of the material exhibiting a given orientation of the crystal lattice, atomic density gradients and zones with different chemical compositions. Nanocrystalline materials show improved properties compared with their conventional polycrystalline counterparts, which can be useful for applications like corrosion and wear resistant coatings, soft magnetic materials for magnetic recording and electrocatalysts for hydrogen evolution and oxidation reactions.

Nanocrystalline materials are produced by various techniques including gas condensation, spray conversion, ball milling, physical vapor deposition, chemical vapor deposition and sputtering techniques. Electrodeposition is a viable, simple operation, versatile and cheaper method to fabricate strong and relatively ductile metallic nanostructures [2]. In electroplating practice, a small concentration of additive molecules is most widely used in the plating bath for controlling the quality of deposit; this leads to significant changes in the properties of the electrodeposits [3-7]. For example, the grain size of nickel deposits can be reduced into nano range (<100 nm) by using additives like coumarin and saccharin. However these additives result in a high concentration of surface active elements such as sulfur and carbon, which can easily segregate to grain boundaries and weaken them. Many plating parameters are involved in the electrodeposition process, such as type of solution, concentration of ions, pH, temperature of the bath, degree of agitation, nature of the substrate, mode of operation, over potential and current density [8].

Watts bath, the most popular nickel electroplating bath, is usually composed of nickel sulfate, nickel chloride and boric acid. Boric acid is an essential ingredient for controlling bath pH and producing smooth and ductile deposits [9]. Japan recently imposed strict environmental protection regulations [10] restricting dumping of waste streams containing boron. Hence in the present investigation, we have made trials on the use potassium citrate [11] as an alternative eco-friendly buffer along with nickel acetate electrolytes.

EXPERIMENTAL DETAILS

The experiments were in triplicate with mild steel metallic foils. Surface preparation prior to deposition is an important factor and can be achieved by mechanical and electrochemical methods, as given in earlier publications [12-14]. The procedure adopted was removal of surface scales using acid dipping, mechanical polishing to get a smooth surface, degreasing with trichloroethylene and final electro cleaning at 4 A dm^{-2} in a solution of sodium carbonate and sodium hydroxide (30 g L^{-1} each). Mild steel metallic foil of 7.5×5 cm^2 and thickness 0.1 cm size was used as cathodes in an electroplating assembly consisting of two 99.99% pure nickel anodes on either side of the cathode. The preset DC regulated power supply with a very low AC ripple was used (APLAB L3230) as source for direct current. The solutions were agitated by magnetic stirrer and temperature was maintained at 50 °C for all experiments. The

†To whom correspondence should be addressed.
E-mail: grsek2004@yahoo.com

nickel plating electrolyte, bath A, consists of nickel sulfate 150 g L^{-1}, potassium chloride 40 g L^{-1} and potassium citrate 30 g L^{-1}; bath B consists of nickel sulfate 150 g L^{-1}, potassium chloride 40 g L^{-1}, potassium citrate 30 g L^{-1}, saccharin sodium salt 0.5 g L^{-1}, 2-butyene 1,4-diol 0.5 g L^{-1} and sodium lauryl sulphate 0.2 g L^{-1}; bath C consists of nickel sulfate 150 g L^{-1}, nickel chloride 40 g L^{-1} and potassium citrate 30 g L^{-1}; and bath D consists of nickel sulfate 150 g L^{-1}, nickel chloride 40 g L^{-1}, potassium citrate 30 g L^{-1}, saccharin sodium salt 0.5 g L^{-1}, 2-butyene 1,4-diol 0.5 g L^{-1} and sodium lauryl sulfate 0.2 g L^{-1}. The plating experiments were performed at different current densities. The substrate cathode was weighed before and after deposition and the cathode current efficiency and rate of build up were calculated using Faraday's law [15,16]. Throwing power was measured using a Haring and Blum cell [17]. This is a rectangular cell consisting of two mild steel metallic foil cathodes of 7.5×5 cm^2 and thickness 0.1 cm size, filling the entire cross section at both ends and one perforated nickel anode of the same size. The latter was placed between the cathodes so that its distance from one of the cathode was one-fifth of its distance from the other. Values of throwing power for different solutions used were calculated using Field's formula:

$$\text{Throwing power (\%)} = \frac{L - M}{L + M - 2} \times 100$$

where M is the metal distribution ratio between the near and far cathode and L is the ratio of the respective distances of the far and near cathodes from the anode.

The microhardness of the electrodeposited nanocrystalline nickel film of about 30 μm thick was calculated by Vickers microhardness (kg mm^{-2}) method using MH6 Everone microhardness tester by an indentation technique at a load of 50 g applied for 15 seconds with a diamond pyramid indenter. Measurements were conducted six times on different areas of each sample and the results were averaged.

Surface Roughness of the electrodeposited nickel film was measured using Surftest SJ-301 surface roughness tester (Mitutoyo, Japan) from the vertical stylus displacement produced during its movement over the surface irregularities. The R_a value gives the average roughness of the surface.

The polarization behavior was studied in the test electrolyte for nickel films of 12 μm thickness. The nickel-deposited mild steel metallic foils were masked to expose 1 cm^2 area on one side. A platinum foil (2.5×2.5 cm^2) and saturated calomel electrode were employed as auxiliary and reference electrodes, respectively; 3.5% sodium chloride was used as test solution and the experiments were performed at 30 °C. The working electrode was introduced into the test solution and allowed to attain a steady potential value. Anodic and cathodic polarization was up to ±200 mV away from the OCP at a scan rate of 1 mVs^{-1}. E_{corr} and i_{corr} values were obtained from the plot of E versus log I curve by Tafel extrapolation method using an electrochemical impedance analyzer Model IM6 with THALES software. The corrosion rate of nickel films were calculated by using this formula [18]:

$$\text{CR (mmpy)} = \frac{K \times I_{corr} \times EW}{\rho}$$

where CR=corrosion rate in mmpy, I_{corr} in μA/cm^2, K is the constant, 3.27×10^{-3} that defines the units for the corrosion rate, EW is the equivalent weight of the metal and ρ is the density of the metal in g/cm^3.

The same three-electrode cell assembly was used for the AC impedance measurements. The nickel-plated samples in the absence and presence of additives were used as working electrode. 3.5% NaCl solution was used as the test solution and the experiments were at 30 °C. The electrochemical impedance measurements were with nickel deposits in 3.5% NaCl solution at open circuit potential in the frequency range 50 mHz-100 kHz. The values of solution resistance (R_s), double layer capacitance (C_{dl}) and charge transfer resistance (R_{ct}) were obtained from Nyquist plots of the real (Z_{Re}) vs imaginary (Z_{im}) components of the impedance. The extent of the corrosion resistance of the coating was determined from the R_{ct} value, using the Stern-Geary equation [19]:

$$I_{corr} = \frac{b_a b_c}{2.303(b_a + b_c)} \frac{1}{R_{ct}}$$

X-ray diffraction patterns were obtained using the X-pert pro powder diffraction system (PE 3040/60) for nickel deposits obtained from various nickel plating baths. The deposits produced in the presence and without additives were studied. The deposits were scanned at 30°-100° (2θ) at a scan rate of 1 degree per minute using CuK_α (λ=1.5405 A°) radiation. The peaks due to the different phases were identified and the corresponding lattice parameters calculated. The crystal size of the nickel deposits was measured by using Scherrer formula [20,21] from the predominant peak.

$$t = \frac{0.9 \times \lambda}{\beta \cos\theta}$$

where 't' is the average size of the crystallites, 0.9 is the Scherrer Constant, 'λ' is the wavelength of the radiation, 'β' is the peak width at half maximum and 'θ' corresponds to the peak position.

The morphology of nickel deposits obtained from different electrolytes was studied by scanning electron microscopy using SEM (Model JEOL-JSM-35 LF) at 25 kV.

RESULTS AND DISCUSSION

1. Cathode Current Efficiency of Nickel Electrolytes

The bath composition and operating parameters (Table 1) were

Table 1. Bath composition and operating conditions

Constituents (g L^{-1})	Bath A	Bath B	Bath C	Bath D
Nickel acetate	150	150	150	150
Potassium chloride	40	40	--	--
Potassium citrate	30	30	30	30
Nickel chloride	--	--	40	40
Saccharin sodium salt	--	0.5	--	0.5
2-Butyene-1, 4-diol	--	0.5	--	0.5
Sodium lauryl sulphate	--	0.2	--	0.2
pH	4	4	4	4
Temperature (°C)	50	50	50	50
Current density (A dm^{-2})	1-5	1-5	1-5	1-5

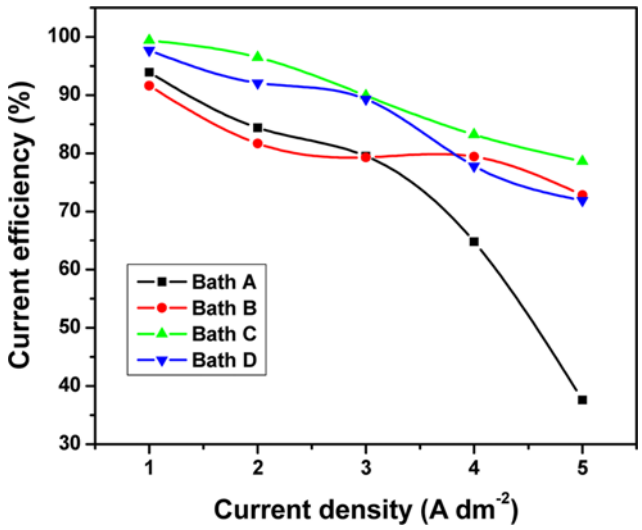

Fig. 1. Current efficiency of various nickel plating solutions obtained at different current densities at 50 °C.

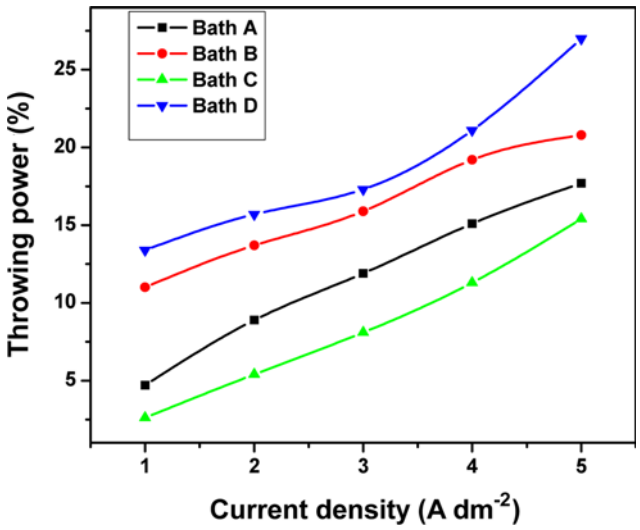

Fig. 2. Throwing power of various nickel plating solutions obtained at different current densities at 50 °C.

selected based on preliminary experiments. Cathode current efficiency measurements were carried out at 50 °C and at different current densities (1-5 A dm^{-2}) for 30 minutes using direct current with different baths A, B, C and D; results are shown in Fig. 1. The curve 'a' results show that for bath A, with KCl and without any brightener, cathode current efficiency and deposition rate steadily decreased with increasing current densities. This decrease in current efficiency may be due to the evolution of hydrogen gas at higher current densities. The nickel film was also deteriorated with increasing current densities. Hence 2-3 A dm^{-2} is more beneficial for producing a smooth, uniform and milky white deposit with acceptable cathode current efficiency 84-79% and the deposition rate of 20.65-29.14 μm h^{-1}.

In curve 'b' is shown the cathode current efficiency for the nickel plating bath with addition of 0.5 gl^{-1} sodium salt of saccharin, 0.5 g L^{-1} of 2-butyene 1,4-diol and 0.02 g L^{-1} of sodium lauryl sulfate (bath B) at 50 °C at different current densities, which show similar trends as for bath A. A smooth uniform bright deposit was observed between 1-3 A dm^{-2}, and above 3A dm^{-2} the deposit becomes streaky. The cathode current efficiency gradually decreases with increasing current densities. It may be attributed to the adsorption of brighteners on the cathode surface which block the active sites of the cathode surface thereby inhibiting electrocrystallization of nickel. Hence, cathode current efficiency decreases with increasing current densities, and thereafter the deposit becomes dark and powdery. 1-3 A dm^{-2} is suitable for producing smooth uniform bright nickel deposit in presence of brighteners.

Curve 'c' represents the cathode current efficiency for bath C containing nickel chloride instead of potassium chloride without any brightener, at 50 °C, and different current densities. From curve 'c' we may see that the current efficiency gradually decreases with increasing current densities. But the current efficiencies are higher compared to the potassium chloride containing bath A. This can be due to increased nickel concentration, thereby increasing the limiting current density. Silvery white deposit was observed between 1-3 A dm^{-2} and satin white deposit was seen between 4-5 A dm^{-2}. Hence, 1-3 A dm^{-2} is sufficient for producing smooth uniform silvery with higher cathode current efficiency.

Curve 'd' shows the cathode current efficiency determined for the nickel plating bath D (using nickel chloride instead of potassium chloride) with addition of 1.0 g L^{-1} sodium salt of saccharin, 0.5 g L^{-1} of 2-butyene-1,4-diol and 0.02 g L^{-1} of sodium lauryl sulfate. A similar trend was observed as in the above case. Mirror bright deposits are obtained at 1-3 A dm^{-2}. In general, nickel chloride containing samples (C and D) exhibited high cathode current efficiency as compared to the potassium chloride containing samples (A and B).

2. Throwing Power of Nickel Electrolytes

In general, throwing power of the baths increases with current density, metal ion concentration in the bath, temperature of the electrolyte, degree of agitation, conductivity of the electrolyte and polarization. Generally, a plating bath having high conductivity is associated with low energy consumption and greater throwing power.

Fig. 2 shows the throwing power values of the nickel plating baths in the absence of additives (baths A and C) and in the presence of additives (baths B and D) calculated using Field's formula under different current densities. In all cases when the current density is increased, throwing power of the bath also increased. This could be attributed to increasing cathodic polarization with increasing current density. The brightener containing baths B and D exhibited higher throwing power as compared to the brightener free baths A and C. This is attributed to the higher cathodic polarization in presence of the added brighteners.

3. Microhardness and Surface Roughness of Nickel Films

The Vickers microhardness, Hv (Kg mm^{-2}), for nickel electrodeposits obtained from various baths at two different current densities is given in Table 2. Deposits obtained in the absence of brighteners (baths A and C) exhibited lower hardness value as compared to that for baths B and D in presence of brighteners. In general, hardness increases with increasing current density. This increase in hardness at higher current density and in presence of brighteners can be attributed to the grain refinement resulting in compact, dense

Table 2. Microhardness of the nickel electrodeposits obtained from various baths at different current densities at 50 °C and at load of 50 g

Bath	Current density (Adm^{-2})	Hardness Hv ($Kg\ mm^{-2}$)
A	1	363
	3	375
B	1	435
	3	515
C	1	409
	3	437
D	1	449
	3	546

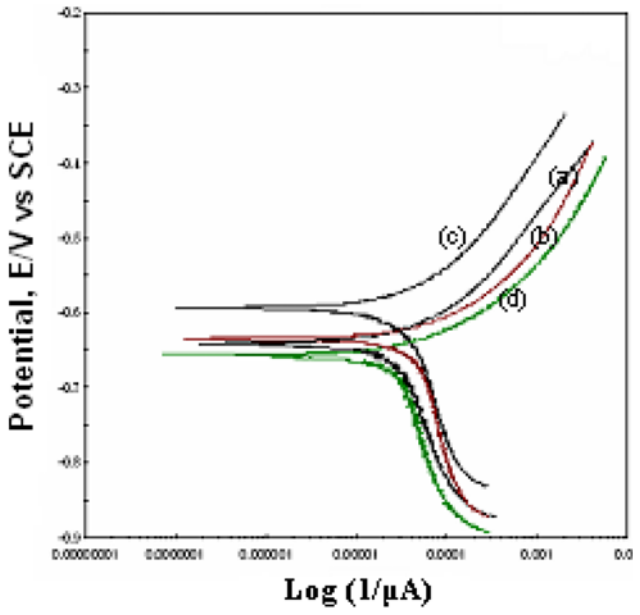

Fig. 3. Potentiodynamic polarization curves for 12 μm thick nickel deposits obtained from different baths in 3.5% NaCl solution at 30 °C.
(a) Bath A (b) Bath B (c) Bath C (d) Bath D

and fine grained deposits.

Among the four baths studied, bath D shows lowest roughness value, Ra of 0.16 μm, as compared to baths A, B and C which have R_a values of 0.42, 0.23 and 0.29, respectively. These roughness values are in order with the visual observation of bright and smooth nature of deposits from the four baths.

4. Potentiodynamic Polarization Studies of Nickel Films

From the electrochemical theory of corrosion, corrosion current densities can be obtained by extrapolating the linear segments of cathodic and anodic Tafel plots. Fig. 3 presents the potentiodynamic polarization curves for nickel deposits of 12 μm thickness obtained from baths A, B, C and D. For nickel deposits from baths A and B, there is no significant change in the corrosion potential, but the deposit obtained from bath A without brighteners exhibited lower corrosion current (Table 3) as compared to the presence of brighteners (bath B). Even though deposits are dense, compact and fine grained, the inclusion or codeposition of sulfur accelerates corrosion rate. Hence, corrosion resistance of the coating decreases as compared to the deposit obtained from bath without brighteners (bath A), which can be understood as an increase in corrosion current due to sulfur inclusion in deposit [22]. On the other hand, the deposit obtained from nickel chloride containing baths (C and D) exhibited lower corrosion current, i_{corr}, as compared to the potassium chloride containing baths A and B. Among all the baths, the deposit obtained from the bath C exhibits the lowest values of i_{corr}. Therefore, the deposit obtained from bath C exhibits the best corrosion resistance, which can be attributed to the compact microstructure. The corrosion rate data obtained using various nickel deposits prepared from different electrolytes are recorded in Table 3. From this data, one can seen that nickel film obtained from bath C displayed lowest corrosion rate and can conclude that nickel film prepared from bath C is dense and fine grain structure.

5. Electrochemical Impedance Spectroscopy (EIS) Studies of Nickel Films

The Nyquist impedance diagram obtained for 12 μm thick nickel deposits obtained using different baths in 3.5% NaCl solution is shown in Fig. 4, and the equivalent circuit fitting the EIS data is shown in Fig. 5. Curves 'a' and 'c' are for nickel deposit from baths A and C without additives and curves 'b' and 'd' for the deposit obtained from baths B and D containing additives.

The impedance plots showed well defined capacitive loop with no evidence of inductive or capacitive loops at lower frequencies. The corrosion of nickel coatings is purely charge transfer controlled, as revealed from the impedance spectrum of perfect semicircle shape [23]. The shape of the impedance spectra supports the assumption that the polarization resistance (R_p) value is the same as the charge transfer resistance (R_{ct}), which is easily estimated on the real impedance axis by extrapolating the impedance trend at the lowest frequencies. The nickel deposit obtained from bath A exhibited higher R_{ct} value 468.2 Ω cm^2 as compared to that from bath B, 408 Ω cm^2. R_{ct} values obtained for nickel deposit obtained from

Table 3. Parameters derived from E vs log I curves for nickel deposits obtained from different nickel baths of 12 μm thickness in 3.5% NaCl solutions at 1 mV s^{-1} at 30 °C

Bath	Corrosion current ($\mu A\ cm^{-2}$)	Corrosion potential (mV versus SCE)	Tafel slopes ($mV\ decade^{-1}$)		Corrosion rate (mmpy)
			Anodic	Cathodic	
A	6.32×10^{1}	−641.8	142	764	0.0679
B	7.64×10^{1}	−636.0	156	843	0.0821
C	4.90×10^{1}	−593.3	118	901	0.0526
D	5.31×10^{1}	−657.0	129	934	0.0570

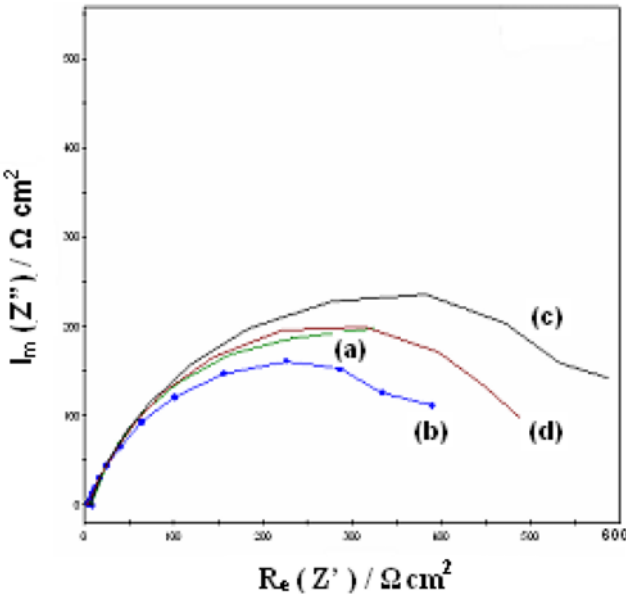

Fig. 4. Equivalent circuit for EIS measurements.

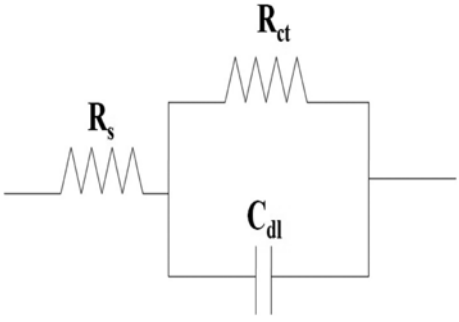

Fig. 5. EIS spectra obtained for 12 μm thick nickel deposits obtained from different baths in 3.5% NaCl solution at 30 °C.
(a) Bath A (b) Bath B (c) Bath C (d) Bath D

the bath C and D are 631.7 and 455.7 Ω cm^2. The charge transfer resistance is inversely proportional to corrosion current; the increase in the protective properties of the coatings is indicated as increasing diameter of the semicircle [24,25]. Hence, among the four deposits studied, the deposit prepared from bath C exhibits the highest corrosion resistance, which is attributed to the highest charge transfer resistance value. In general, the conditions that were favorable for good nickel deposition were characterized by a single loop at high frequency with low capacitance and high charge transfer resistance [26].

6. X–ray Diffraction and Crystal Size Measurements of Nickel Films

Crystallographic studies by X-ray diffraction technique of nickel electrodeposits prepared from different baths at 3 A dm^{-2} are shown in Fig. 6(a)-6(d). The crystal size was calculated from the predominant (111) plane in all samples using Scherrer formula (Table 4). In the XRD pattern of nickel electrodeposits produced from bath A without additives (Fig. 6(a)), the reflection of (111) plane was more predominant and other peak intensities are less. The (111) plane is the preferred orientation normal to the surface due to energy

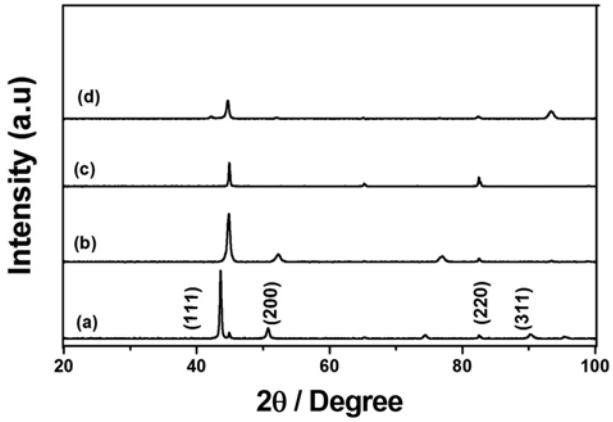

Fig. 6. XRD pattern for nickel deposits obtained from various baths at 3 A dm^{-2}.
(a) Bath A (b) Bath B (c) Bath C (d) Bath D

Table 4. Crystal size of nickel deposits obtained from different baths at various current densities

Bath	Current density (Adm^{-2})	2θ Value	FWHM value	Plane	Crystal size (nm)
A	3	44.8243	0.3178	(111)	27.07
B	3	44.7721	0.4015	(111)	21.42
C	3	44.6461	0.4015	(111)	21.41
D	3	44.7598	0.4684	(111)	18.36

considerations, but the fiber texture is weakened with grain growth, and grains with orientations other than (111) are also present [27]. On the other hand, the cathode polarization is great enough to eliminate faster-growing lattice (111) planes, which have lowest lattice surface energy, developed parallel to the substrate.

In Fig. 6(b) for the nickel electrodeposits obtained from bath B containing additives also, (111) reflection is much greater than that of any of the other reflections (200), (220) and (311). That is, most of the crystals in the polycrystalline substrate have their (111) planes parallel to surface and the 2θ position of the (200) plane is shifted as compared to that without brighteners. The preferred orientation of (111) plane is due to Ni^{2+} cations that are adsorbed on growth centers with a (100) texture with the result that growth occurs in the (111) direction. Furthermore, the proton adsorption may give rise to similar effects to those arising when organic additives consume cathodic hydrogen [28]. It is known that such organic additives give rise to electrodeposits of nickel with (111) growth directions [29].

In Fig. 6(c) the X-ray diffraction pattern for deposit from bath C shows that the (111) fiber texture was more predominant with the (111) plane intensities significantly increased and (200) plane was vanished. In general, peak intensity increases with decreasing the grain size. Fig. 6(d) shows the deposits obtained from the bath D with predominant (111) reflection and again the (200) plane was disappeared. Moreover, the crystal size was significantly reduced. When the overpotential is very high, the rate of nucleation is generally so fast that crystal growth in any preferred lattice direction may be difficult and grain becomes finer. Therefore, the deposit

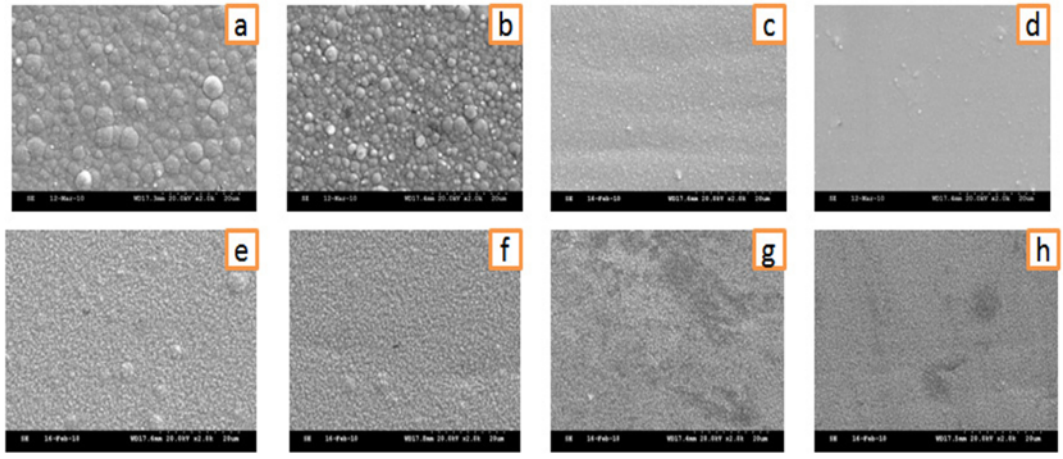

Fig. 7. SEM photograph of nickel deposits obtained from various baths and different current densities.
(a) Bath A, 1 A dm^{-2} (b) Bath A, 3 A dm^{-2} (c) Bath B, 1 A dm^{-2} (d) Bath B, 3 A dm^{-2} (e) Bath C, 1 A dm^{-2} (f) Bath C, 3 A dm^{-2} (g) Bath D, 1 A dm^{-2} (h) Bath D, 3 A dm^{-2}

should have a random crystal structure. Preferential growth modes in electrocrystallized nickel arise due to the inhibition of other growth modes. The most common inhibitors to affect the growth process are hydrogen gas, adsorbed hydrogen atoms or nickel hydroxide at the electrode surface.

7. Surface Morphology of Nickel Films

SEM micrographs of nickel electrodeposits obtained from bath A at different current densities are shown in Fig. 7(a) and 7(b). At 1 A dm^{-2}, the hemispherical grain structures are randomly arranged over the entire area of the surface (Fig. 7(a)). Fig. 7(b) shows that at 3 A dm^{-2} it had resulted in reduction in grain size slightly and the random surface morphology was enlarged to homogeneous hemispherical surface morphology. These variations can be explained in terms of the model of nucleation and growth of crystals in which growth from existing nuclei is favored at low current densities. While at high current densities massive nucleation is the predominant effect, thus giving rise to small grains small [30]. Fig. 7(c) and (d) show SEM micrographs of the nickel electrodeposits obtained from bath B in presence of brighteners at 1 A dm^{-2} and 3 A dm^{-2}. Fig. 7(c) shows that addition of brighteners produced a different surface morphology. The hemispherical grain structure was reduced to fine grain size and without pores on the surface. It was characterized by clusters of non-uniform large nodules growing on the surface. In Fig. 7(d) at 3 A dm^{-2}, the grain size becomes still smaller. Fig. 7(e) and 7(f) show SEM micrographs of the nickel electrodeposits obtained from bath C in the absence of brighteners. Fig. 7(e) at 1 A dm^{-2} shows the absence of additive in the nickel layer that consists of round shaped colony like morphology. When the current density increases to 3 A dm^{-2} (Fig. 7(f)), there is a change in the surface morphology but decrease in grain size. It is expected that the grain size of the nickel films decreases with increasing the current density, because an increase in the current density results in a higher overpotential that increases the nucleation rate.

Fig. 7(g) and 7(h) show SEM micrographs of nickel electrodeposits obtained from bath D in the presence of brighteners at 1 A dm^{-2} and 3 A dm^{-2}. Fig. 7(g) shows that deposit from bath with addition of brighteners shows a different surface morphology. The round shaped colony like structure was refined to produce a fine grained surface morphology. When current density increases to 3 A dm^{-2} (Fig. 7(h)), the grain size becomes still smaller. In fact, the energy of grain nucleus formation depends on the cathodic overpotential. In our case, brighteners can increase cathodic overpotential and reduce the energy of nucleus formation, consequently refining the grain size of the nickel films [31].

CONCLUSIONS

Smooth and adherent deposits of nickel are obtained from acetate-based electrolyte without and with brighteners with high cathode efficiency, agreeable throwing power and high hardness value. Potentiodynamic polarization studies reveal that the deposits obtained in the absence of additives exhibit higher corrosion resistance compared to the deposits obtained from additive-containing baths. Among these baths studied, the nickel deposits obtained from the nickel chloride containing bath C have the highest corrosion resistance, which can be correlated with its dense and fine grained structure. This is further confirmed by electrochemical impedance measurements that show that the deposit obtained from the nickel chloride containing bath C exhibited highest R_{ct} value, indicating the highest corrosion resistance.

X-ray diffraction studies reveal that the deposits obtained from baths containing different additives show the characteristic XRD pattern of nickel with (111) plane more predominant in all the cases. The crystal size calculation based on XRD data indicates that the deposits obtained from all the baths are 27.07-18.36 nm range in grain size. SEM photographs show that the deposit obtained in the absence of additive has a uniform cluster of hemispherical grain structures, whereas the deposit obtained from the additive containing baths has dense, fine grained, pin-hole free structure.

REFERENCES

1. F. A. Lowenheim, *Modern electroplating*, New York, McGraw-Hill (1978).

2. F. Ebrahimi, D. Kong, T. E. Matthews and Q. Zhai, *Processing and Fabrication of Advanced Materials VII Ed*., Warrendale, PA, TMS Publication, 509 (1988).
3. S. Trasatti, *Electrochim. Acta*, **37**, 2137 (1992).
4. T. C. Franklin. *Plat. Surf. Finish*, **81**, 62 (1994).
5. L. Oniciu and L. Muresan, *J. Appl. Electrochem.*, **21**, 565 (1991).
6. W. Plieth, *Electrochim. Acta*, **37**, 2115 (1992).
7. R. Sekar, C. Eagammai and S. Jayakishnan, *J. Appl. Electchem.*, **40**, 49 (2010).
8. H. D. Merchant, *Defect structure, morphology and properties of deposits*, Warrendale, PA, TMS Publication 1 (1995).
9. J. K. Dennis and T. E Such, *Nickel and Chromium plating*, London, Newnes-Butterworths, 163 (1972).
10. Notification of the Director General of the Environment Agency in Japan, **2**, 22 (1999).
11. T. Doi, K. Mizumoto, S. Tanaka and T. Yamashita, *Met. Finish*, **102**, 26 (2004).
12. R. Sekar and S. Jayakrishnan, *Plat. Surf. Finish*, **92**, 58 (2005).
13. R. Sekar, C. Kala and RM. Krishnan, *Trans. Inst. Met. Finish*, **80**, 173 (2002).
14. R. Sekar, RM. Krishnan and V. S. Muralidharan, *Trans. Inst. Met. Finish*, **82**, 164 (2004).
15. H. Silman, G. Isserlis and A. F. Averill, *Protective and decorative coatings for metals*, Teddington England, Finishing Publications Ltd. (1978).
16. R. Sekar and S. Jayakishnan, *J. Appl. Electrochem*., **36**, 591 (2006).
17. B. E. Conway and JO'M Bockris, *Plating*, **46**, 371 (1959).
18. ASTM-G102-89 Standard Practice for calculation of Corrosion Rates and related information from Electrochemical Measurements, **03.02** 435 (2001).
19. M. Stern and A. L. Geary, *J. Electrochem. Soc*., **104**, 56 (1957).
20. B. D. Cullity, *Elements of X-ray diffraction*, USA, Addison Wesley (1967).
21. H. P. Klug and L. Alexander, *X-ray diffraction procedures for polycrystalline and amorphous materials*, New York, Wiley (1980).
22. G. Gyawali, K. Hamal, B. Joshi, A. Rajbhandari and S. W. Lee, *Mater. Lett.*, **126**, 228 (2014).
23. F. Mansfield, W. Kendig and S. Tasi, *Corrosion*, **38**, 570 (1982).
24. S. Survilline, A. Cesuniene and R. Juskena, *Trans. Inst. Met. Finish*, **82**, 185 (2004).
25. S. Survilline, V. Jasualaitiene and A. Cesuniene, *Trans. Inst. Met. Finish*, **83**, 130 (2005).
26. M. Holm and T. J. O' Keefe, *J. Appl. Chem.*, **83**, 1125 (2000).
27. L. P. Gai, R. Mitra and J. R .Weertman, *Pure. Appl. Chem*., **74**, 1519 (2002).
28. J. Amblard, I. Epelboin, M. Froment and G. Maurin, *J. Appl. Electrochem.*, **9**, 223 (1979).
29. A. G. Mc Cormack, M. J. Pomeroy and V. J. Cunnane, *J. Electrochem. Soc*., **150**, 356 (2003).
30. A. Ibanez and E. Fatas, *Surf. Coat. Technol.*, **191**, 7 (2005).
31. E. Budevski, G. Staikov and W. J. Lorenz, *Electrochim. Acta*, **45**, 2259 (2000).